Measurement of angstrom-level laser induced protrusion using touchdown in heat-assisted magnetic recording

Qilong Cheng,[1, a)] Haoyu Wang,[2] Siddhesh V. Sakhalkar,[1] and David B. Bogy[1]
[1)] *University of California at Berkeley, Berkeley, California 94720, USA.*
[2)] *Shanghai Jiao Tong University, Shanghai 200240, China.*

(Dated: 17 September 2020)

In heat-assisted magnetic recording (HAMR), a laser is employed above the read-write transducer to provide energy to the media, lowering its coercivity. However, the laser also brings thermal energy diffusion inside the slider and induces an extra angstrom-level protrusion, which we call laser induced protrusion (LIP). The LIP needs to be taken into consideration in HAMR due to the significance of head-media spacing. This paper focuses on laser heating in millisecond timescale during flying in the HAMR conditions. When the laser is turned ON for milliseconds, the LIP forms in the short term ($\sim \mu$s) and fly height change (FHC) happens in the long term ($\sim$ ms) due to crown/camber change, resulting in a smaller touchdown power (TDP). Thus, the touchdown power change (ΔTDP) is measured and the LIP is isolated using the time constants. A component-level HAMR stage is used to study the effects of laser-on time, laser current and linear velocity on the ΔTDP. The experimental results show that the FHC needs $\sim$ 28 ms to reach steady state and that the protrusion size presents a two-stage linear relation with the laser current separated by a threshold. The LIP size reduces by around half when operating from 12 m/s to 24 m/s.

As data generated worldwide are growing explosively, it is crucial to increase areal density of traditional storage devices to satisfy the requirements. The industry has reached a consensus that heat-assisted magnetic recording (HAMR) is probably the most promising technology for hard disk drives (HDDs) to improve the areal density over 1 Tb/in^2.[1,2] To realize this higher storage density, the head-disk interface (HDI) spacing should be less than 2-3 nm. Thus, a thermal fly-height control (TFC) element is utilized to induce a microscale thermal protrusion to decrease the HDI spacing at the head-write transducer. It is also required that magnetic materials with smaller grain size are used for the media, but data writing is challenged because of their higher coercivity.[3,4] To assist the writing process, a laser is introduced in HAMR as shown in Figure 1. The laser travels through a waveguide element and a near field transducer (NFT) element to locally produce a nanoscale hot spot on the rotating disk, lowering the coercivity of the magnetic layer.[2,5] The laser diode has an efficiency of around 50% and half of the input energy heats the whole slider body, leading to crown/camber change.[6] The rest of the energy that passes through the waveguide is partially absorbed by the head carbon overcoat, forming an extra localized angstrom-level protrusion, which we call laser induced protrusion (LIP). The LIP needs to be considered in the HDI spacing control and compensated for during flying in the HAMR conditions.[7] The LIP may also cause material failure, leading to the degradation of the HDD performance.[8]

In the previous studies, HAMR reliability issues such as heat transfer and lubricant transfer were broadly investigated.[9–15] Only several studies focused on the LIP at the head surface. An atomic force microscope (AFM) technique was used by Schreck *et al.* to measure the NFT protrusion in the static condition and the result was combined with modelling to extend to the flying condition.[6,16] A burnish method was utilized by Zhang *et al.* to characterize the LIP through contact with the rotating disk and AFM topography scans.[17] Xiong *et al.* came up with a timescale-based burst writing method to evaluate the NFT protrusion and the spacing in HAMR.[18] The LIP has hitherto been measured based on burnishing or readback signal. In this paper, we propose a touchdown-based scheme to study the LIP.

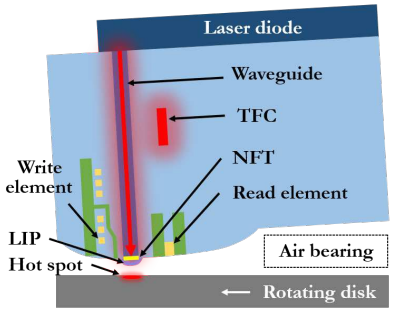

FIG. 1. Schematic diagram (not to scale) of HAMR head-disk interface

When the laser is switched from OFF to ON, the TFC touchdown power (TDP), indicated by an acoustic emission (AE) sensor, decreases due to spacing loss that results from laser heating. The TFC touchdown power change (ΔTDP) is measured to study the LIP. We focus on the millisecond timescale effect of laser heating during flying, and the measured ΔTDP is the overall outcome

[a)] Email: qlcheng@berkeley.edu

of the localized protrusion (LIP, time constant $\tau_1 \sim \mu s$) and the fly height change (FHC, time constant $\tau_2 \sim$ ms, not drawn in Figure 1).[18] The effects of laser-on time, laser current and linear velocity are investigated.

In the experiments, a component-level HAMR test stage was built as shown in Figure 2. HAMR media with glass substrate and HAMR heads that contain the waveguide element ($\sim$ 500 nm, without NFT) are used since NFT is not available to us. In the heads, the thermal fly-height control (TFC) element and the laser element are energized to perform the touchdowns in the head-disk interface. The touchdowns are indicated by an acoustic emission (AE) sensor that is attached to the slider fixture.

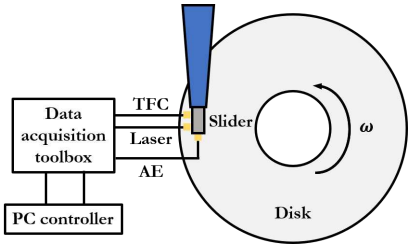

FIG. 2. Schematic diagram of the experimental setup

In each experiment, the laser is biased using a constant DC current and the TFC power is increased in steps (0.25 mW) to perform the touchdowns. The resolutions are 0.1 mA and 0.01 mW for the laser current and the TFC power. Figure 3 shows a typical implementation of the TFC power and the laser current. In each sampling period, the laser element is turned OFF in the first half of the sampling time (laser-off regime) and turned ON in the other half (laser-on regime). When the laser element is turned ON, the laser passes through the waveguide and directly shines on the rotating media. The TDPs measured in the laser-off regime and the laser-on regime are different due to the laser, and hence, the difference ΔTDP is measured to study the LIP. Since the TFC power and AE signal are measured simultaneously in each sampling period, this implementation ensures identical initial conditions for both the laser-off regime and the laser-on regime, regardless of smear from the laser heating or wear from overpush touchdowns. Then different flying parameters such as laser-on time, laser current and linear velocity are controlled to study their effects.

Figure 4 shows the result of AE signals at different TFC powers when flying at the linear velocity V = 18 m/s. Notice that the left and right halves, divided by the vertical red dash line in the sub-figures, correspond to the laser-off regime and the laser-on regime as demonstrated in Figure 3. When the TFC power is 168.90 mW, the AE signal remains at its baseline value in both of the two regimes, so the head flies normally with the laser OFF and ON. Then, when the TFC power is 170.90 mW or

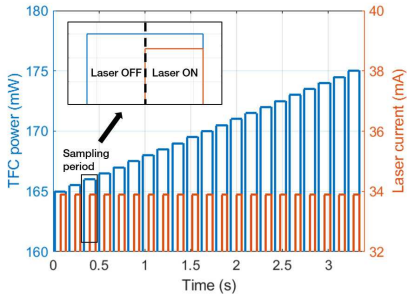

FIG. 3. Sampling patterns used in the experiments (inset: zoom in of one sampling period)

173.90 mW, the appearance of the spikes in the right half indicates that contact occurs in the laser-on regime, but no contact is observed in the laser-off regime. At these two TFC powers, the head keeps flying without the laser, but turning on the laser induces spacing change (the LIP and the FHC), resulting in contact between the head protrusion and the rotating disk. Furthermore, Figure 4 (b) does not show the contact until the laser remains ON for tens of milliseconds, which matches the time constant τ_2 of the FHC. When the TFC power increases to 175.40 mW, 175.90 mW and 176.90 mW, the AE signals also indicate contact in the laser-off regime as well as in the laser-on regime. At these three TFC powers, contact occurs even without the laser because the TFC protrusions alone are too large compared to the head-disk spacing.

Figure 5 plots the root mean square (RMS) of the AE signal versus the TFC power in the laser-off regime and the laser-on regime, which are also called touchdown curves, at the same flying conditions as in Figure 4. The two curves are measured simultaneously in each sampling period, so the only variable between them is the laser OFF/ON. The TDP is defined as the TFC power where the AE RMS signal ramps up beyond 105% of its baseline value.[19] With the laser turned ON, the TDP decreases by several milliwatts due to the laser. In the following experiments, the ΔTDP is measured and the LIP is isolated using the time constants. Note that three states are observed in both the touchdown curves, which are termed "flying state", "bouncing state" and "surfing state".[20]

Assume that the transient reponses of the LIP and the FHC can be described as

$$\begin{aligned} P_{\mathrm{LIP}} &= A_1(1-e^{-\frac{t}{\tau_1}}) \approx A_1 \quad (t \sim ms) \\ P_{\mathrm{FHC}} &= A_2(1-e^{-\frac{t}{\tau_2}}) \\ \Delta\mathrm{TDP} &= -A_2 e^{-\frac{t}{\tau_2}} + A_1 + A_2 \end{aligned} \tag{1}$$

where P_{X} refers to the ΔTDP induced by the factor X and A_1, A_2, τ_1, τ_2 are the amplitudes and the time constants of the LIP and the FHC, respectively. Figure 6

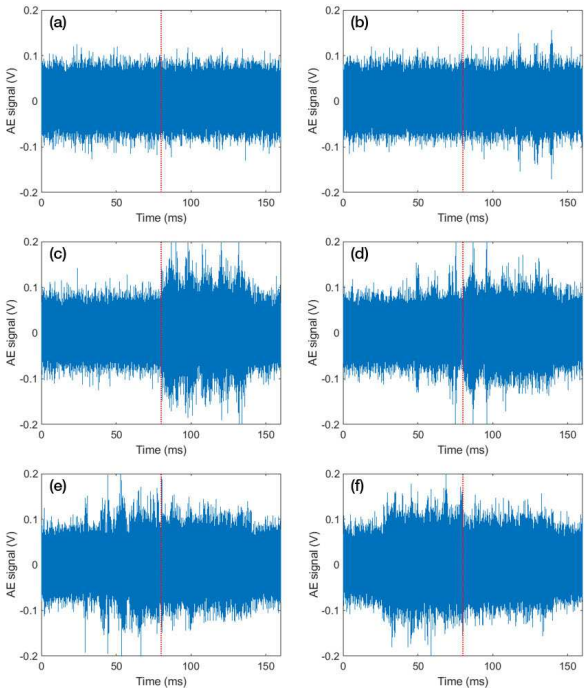

FIG. 4. AE signals at TFC powers (a) 168.90 mW (b) 170.90 mW (c) 173.90 mW (d) 175.40 mW (e) 175.90 mW (f) 176.90 mW when the laser current is 33.9 mA

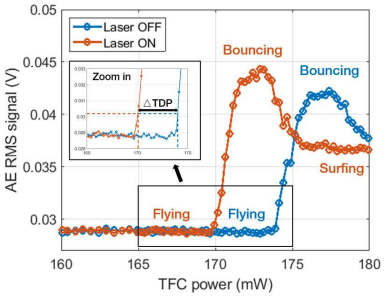

FIG. 5. The result of ΔTDP due to laser heating (inset: zoom in of ΔTDP)

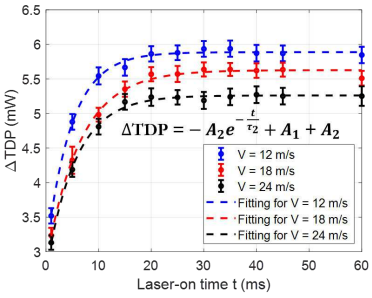

FIG. 6. Relationship between the ΔTDP and the laser-on time when the laser current is 40.8 mA

shows the relationship between the ΔTDP and the laser-on time with the linear velocity of 12, 18 and 24 m/s and the laser current of 40.8 mA, along with the exponential fittings. The fitting parameters can be found in Table I. Figure 6 shows that the ΔTDP increases with the laser-on time, which matches the transient development of the LIP and the FHC at the surface of the recording head.[18] Table I indicates that the LIP and the FHC have similar contributions, and that the FHC time constant τ_2 is $\sim$ 5.6 ms in average. Thus, the ΔTDP needs $\sim$ 28 ms to

TABLE I. Fitting parameters for the transient ΔTDP

Velocity (m/s)	A_1 (mW)	A_2 (mW)	τ_2 (ms)
12	2.979	2.908	4.799
18	2.829	2.797	6.513
24	2.698	2.563	5.556

reach steady state in all three cases. Actually the laser also results in a disk protrusion, however, which can be neglected because it is much smaller compared to the LIP and has a time constant in nanoseconds.[6]

Figure 7 shows the relationship between the ΔTDP and the laser current at the same velocities. The laser-on time is fixed at 60 ms, which is long enough for the ΔTDP to become stable according to the experimental results in Figure 6. The ΔTDP has a two-stage linear relation with the laser current, which matches well with the previous calibration of the optical power with the laser current as shown in Figure 7 inset.[21] The LIP and the FHC are formed by the absorption of the output laser power and the thermal diffusion in the slider. Hence, the ΔTDP caused by the laser is supposed to be proportional to the output laser power (optical power), which presents two slopes versus the laser current before/after the current threshold I_{th}.

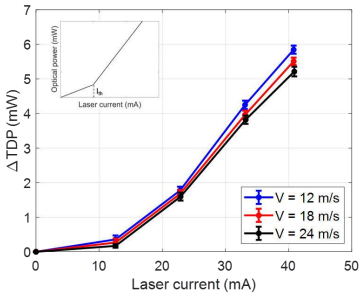

FIG. 7. Relationship between the ΔTDP and the laser current (inset: the optical power versus the laser current[21])

So far, the TFC touchdown power change (ΔTDP) has been used to evaluate the LIP, but the TFC efficiency (nm/mW) depends on the linear velocity in terms of absolute spacing (nm). Simulations based on CMLAir are performed using a similar slider.[22] Figure 8 shows the simulation results of minimum flying height versus TFC power at the three velocities. Since the ΔTDP is measured using the touchdown scheme, the TFC efficiency near disk proximity, namely close to contact, is important. A constant TFC efficiency near contact is assumed. The boxes in Figure 8 show that the TFC efficiency is 0.0517, 0.0346 and 0.0281 nm/mW near disk proximity at V= 12, 18, 24 m/s, respectively. When flying at a higher velocity, the same amount of the TFC power change corresponds to a smaller spacing change due to stronger air cooling and air pressure.[7]

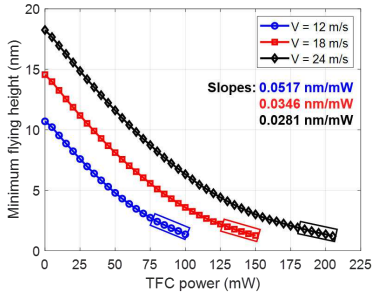

FIG. 8. The simulation results of minimum flying height versus TFC power

Using the TFC efficiency (nm/mW) from the simulations, the ΔTDP (mW) can be converted into space change (nm), which arises from the LIP and the FHC. The LIP's portion is isolated assuming a constant ratio A_1/A_2 at the same velocity. Figure 9 shows the separated LIP size versus the laser current. In the case of 40.8 mA laser current, the ΔTDPs measured in the three cases are 5.85, 5.51 and 5.21 mW with standard deviation ∼ 0.12 mW as shown in Figure 7, which can be converted by the TFC efficiency into 3.02, 1.91 and 1.46 Å with standard deviation ∼ 0.05 Å. Considering the ratios A_1/A_2 in Table I, the separated LIP sizes are 1.53, 0.96, 0.75 Å for the three velocities. Therefore, the LIP reduces by around half when the linear velocity increases from 12 m/s to 24 m/s, which is also caused by the stronger air cooling and air pressure.

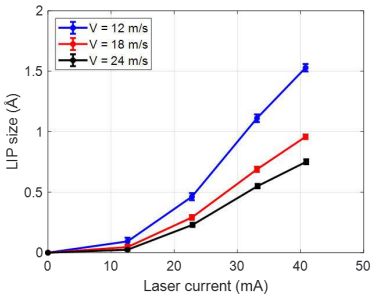

FIG. 9. Relationship between the LIP size and the laser current

In this paper, the touchdown-based experiments are conducted to quantify the spacing change due to the laser heating in millisecond timescale during flying. The spacing change originates from the angstrom-level LIP and

the FHC, which can be separated using their time constants in μs and ms. The experimental results show that the FHC needs $\sim$ 28 ms to become stable and that the LIP presents a two-stage relation versus the laser current. As the operating linear velocity increases from 12 m/s to 24 m/s, the LIP size reduces by around half.

The work was supported by Computer Mechanics Laboratory at Department of Mechanical Engineering, UC Berkeley. We thank Erhard Schreck, Robert Smith, Sukumar Rajauria and Tan Trinh of Western Digital Corporation for supplying the components and providing insightful discussions.

DATA AVAILABILITY

The data and material that support the findings of this study are available from the corresponding author upon reasonable request.

[1]M. H. Kryder, E. C. Gage, T. W. McDaniel, W. A. Challener, R. E. Rottmayer, G. Ju, Y.-T. Hsia, and M. F. Erden, "Heat assisted magnetic recording," Proceedings of the IEEE **96**, 1810–1835 (2008).
[2]W. Challener, C. Peng, A. Itagi, D. Karns, W. Peng, Y. Peng, X. Yang, X. Zhu, N. Gokemeijer, Y.-T. Hsia, *et al.*, "Heat-assisted magnetic recording by a near-field transducer with efficient optical energy transfer," Nature photonics **3**, 220–224 (2009).
[3]D. Weller and A. Moser, "Thermal effect limits in ultrahigh-density magnetic recording," IEEE Transactions on magnetics **35**, 4423–4439 (1999).
[4]M. A. Seigler, W. A. Challener, E. Gage, N. Gokemeijer, G. Ju, B. Lu, K. Pelhos, C. Peng, R. E. Rottmayer, X. Yang, *et al.*, "Integrated heat assisted magnetic recording head: Design and recording demonstration," IEEE Transactions on Magnetics **44**, 119–124 (2007).
[5]L. Pan and D. B. Bogy, "Heat-assisted magnetic recording," Nature Photonics **3**, 189–190 (2009).
[6]E. Schreck, D. Li, S. V. Canchi, L. Huang, G. P. Singh, B. Marchon, H. J. Richter, B. Stipe, and M. Staffaroni, "Thermal aspects and static/dynamic protrusion behaviors in heat-assisted magnetic recording," IEEE transactions on magnetics **50**, 126–131 (2014).
[7]S. Xiong, R. Smith, J. Xu, S. Nishida, M. Furukawa, K. Tasaka, K. Kuroki, Y. Yoon, N. Wang, S. Canchi, *et al.*, "Spacing control in heat-assisted magnetic recording," IEEE Transactions on Magnetics **55**, 1–6 (2018).
[8]C. Zhong, P. Flanigan, N. Abadía, F. Bello, B. D. Jennings, G. Atcheson, J. Li, J.-Y. Zheng, J. J. Wang, R. Hobbs, *et al.*, "Effective heat dissipation in an adiabatic near-field transducer for hamr," Optics express **26**, 18842–18854 (2018).
[9]H. Wu and D. Bogy, "Use of an embedded contact sensor to study nanoscale heat transfer in heat assisted magnetic recording," Applied Physics Letters **110**, 033104 (2017).
[10]Y. Hu, H. Wu, Y. Meng, Y. Wang, and D. Bogy, "Head flying characteristics in heat assisted magnetic recording considering various nanoscale heat transfer models," Journal of Applied Physics **123**, 034303 (2018).
[11]S. V. Sakhalkar and D. B. Bogy, "Viscoelastic lubricant deformation and disk-to-head transfer during heat-assisted magnetic recording," IEEE Transactions on Magnetics **55**, 1–6 (2018).
[12]S. Sakhalkar, Q. Cheng, A. Ghafari, Y. Ma, and D. Bogy, "Numerical and experimental investigation of heat transfer across a nanoscale gap between a magnetic recording head and various media," Applied Physics Letters **115**, 223102 (2019).
[13]Y. Ma, A. Ghafari, Y. Wu, and D. Bogy, "A study of the nanoscale heat transfer in the hdd head–disk interface based on a static touchdown experiment," IEEE Transactions on Magnetics **56**, 1–7 (2020).
[14]Q. Cheng, S. Sakhalkar, A. Ghafari, Y. Ma, and D. Bogy, "Dependence of nanoscale heat transfer across a closing gap on the substrate material and ambient humidity," Applied Physics Letters **116**, 213102 (2020).
[15]N. Tagawa, H. Tani, Y. Uesaraie, S. Koganezawa, and R. Lu, "Experimental study of lubricant depletion induced by pulsed laser irradiation heating in heat-assisted magnetic recording," Microsystem Technologies **26**, 5–10 (2020).
[16]D. Li, M. Staffaroni, E. Schreck, and B. Stipe, "A new afm-based technique to detect the nft protrusion on hamr head," IEEE transactions on magnetics **49**, 3576–3579 (2013).
[17]Z. Zhang, K. Liu, E. X. Jin, M. M. Dovek, J. D. Kiely, O. Nakada, P. K. Wong, V. M. F. Chiah, and X. M. Liu, "Characterization of laser-induced protrusion in hamr by the burnish method," IEEE Transactions on Magnetics **52**, 1–6 (2015).
[18]S. Xiong, R. Smith, J. Xu, S. Nishida, M. Furukawa, K. Tasaka, K. Kuroki, Y. Yoon, N. Wang, S. Canchi, *et al.*, "Setting write spacing in heat assisted magnetic recording," IEEE Transactions on Magnetics **54**, 1–7 (2018).
[19]Y. Ma, *Study of Dynamics and Nanoscale Heat Transfer of Head Disk Interface in Hard Disk Drives*, Ph.D. thesis, UC Berkeley (2018).
[20]Y.-K. Chen, J. Zheng, and D. B. Bogy, "Light contact and surfing state dynamics of air bearing sliders in hard disk drives," Applied physics letters **100**, 243104 (2012).
[21]J. Wang, K. Ma, Z. Ye, W. E. Wong, G. Guo, and Y. Wang, "Hamr writing process model-based compensation of laser-induced transients," IEEE Transactions on Magnetics **53**, 1–7 (2016).
[22]S. Sakhalkar, Q. Cheng, A. Ghafari, and D. Bogy, "Investigation of heat transfer across a nanoscale air gap between a flying head and a rotating disk," Journal of Applied Physics **128**, 084301 (2020).